Circulation around a Constrained Curve: An Alternative Analysis Tool for Diagnosing the Origins of Tornado Rotation in Numerical Supercell Simulations

ROBERT DAVIES-JONES^a AND PAUL M. MARKOWSKI^b

^a NOAA/National Severe Storms Laboratory, Norman, Oklahoma
^b Department of Meteorology and Atmospheric Science, The Pennsylvania State University, State College, Pennsylvania

(Manuscript received 25 January 2021, in final form 18 June 2021)

ABSTRACT: Fine-resolution computer models of supercell storms generate realistic tornadic vortices. Like real tornadoes, the origins of these virtual vortices are mysterious. To diagnose the origin of a tornado, typically a near-ground material circuit is drawn around it. This circuit is then traced back in time using backward trajectories. The rate of change of the circulation around the circuit is equal to the total force circulation. This circulation theorem is used to deduce the origins of the tornado's large vorticity. However, there is a well-known problem with this approach; with staggered grids, parcel trajectories become uncertain as they dip into the layer next to the ground where horizontal wind cannot be interpolated. To circumvent this dilemma, we obtain a generalized circulation theorem that pertains to any circuit. We apply this theorem either to moving circuits that are constrained to simple surfaces or to a "hybrid" circuit defined next. Let A be the horizontal surface at one grid spacing off the ground. Above A the circuit moves as a material circuit. Horizontal curve segments that move in A with the horizontal wind replace segments of the material circuit that dip below A. The circulation equation for the modified circuit includes the force circulation of the inertial force that is required to keep the curve segments horizontal. This term is easily evaluated on A. Use of planar or circular circuits facilitates explanation of some simple flows. The hybrid-circuit method significantly improves the accuracy of the circulation budget in an idealized supercell simulation.

KEYWORDS: Tornadogenesis; Supercells; Tornadoes; Vorticity

1. Introduction

Based on a maximum tangential wind of $100\,\mathrm{m\,s^{-1}}$ at a core radius of 100 m, the vertical vorticity in the core of a strong tornado is estimated to be 2 s⁻¹. The corresponding estimate for the circulation at the radius of maximum tangential velocity is $6.3 \times 10^4 \,\mathrm{m}^2 \,\mathrm{s}^{-1}$. How such large values of vorticity and circulation develop on the scale of a tornado core is still undecided (Davies-Jones et al. 2001; Davies-Jones 2015). Even though some fine-resolution computer simulations of supercell storms (without Earth's background vorticity) generate realistic tornado-like vortices (Orf et al. 2017), the origins of these vortices are difficult to decode, as foretold by Rotunno (1986). In many studies, diagnostic calculations based on circulation are performed on fields generated either by computer simulations of supercells (e.g., Rotunno and Klemp 1985; Davies-Jones and Brooks 1993; Adlerman et al. 1999) or by Doppler-radar analyses of actual supercells (e.g., Markowski et al. 2012). Typically, a small material horizontal circuit is drawn at some time t_1 around the maximum of vertical vorticity at a low level in the storm. By calculating backward trajectories, this circuit is taken backward to an earlier reference time t_0 . By Kelvin's theorem (Dutton 1986, p. 368), the barotropic part of the circulation does not change and so is equal to the initial circulation at t_0 . The total circulation generally changes significantly over long intervals $[t_0, t_1]$ as a result of torques (Shapiro 1972).

Davies-Jones's status: Emeritus.

Corresponding author: Robert Davies-Jones, bobdj1066@ yahoo.com

The rate of change of the circulation is equal to the sum of the force circulations, i.e., to the sum of the line integrals of the tangential forces acting around the circuit (Dutton 1986, p. 372). The baroclinic and frictional force circulations account for the increase in circulation in the interval $[t_0, t_1]$ and most of the total circulation at t_1 (Rotunno and Klemp 1985; Davies-Jones and Brooks 1993; Trapp and Fiedler 1995; Adlerman et al. 1999; Dahl et al. 2014; Dahl 2015; Roberts et al. 2016, 2020; Roberts and Xue 2017; etc.).

Calculating the circulation around a material circuit that is drawn horizontally around a near-ground vorticity maximum and then tracked backward using saved data to a much earlier time is susceptible to several errors including interpolation and extrapolation ones. The backward trajectories used to trace the circuit can be clearly erroneous, such as when they cross frontal boundaries dividing air masses (Dahl et al. 2012) or when parcels remain trapped in the vortex (Markowski et al. 2012, p. 2918). The circuit should be recoverable by running forward trajectories from the earlier time. However, this is not the case if the numerical trajectory scheme does not satisfy time-reversal symmetry adequately. Since the flow is 3D and convergent (i.e., divergent in backward time), the length of the circuit gets very large and becomes very convoluted (Markowski and Richardson 2014). Because trajectories can be chaotic (Dombre et al. 1986), the curve may resemble a fractal and thus have a length (Mandelbrot 1982) and circulation around it that may converge poorly with progressively finer model resolution.

Almost all 3D numerical models of clouds use staggered grids. In these models the vertical wind vanishes at the ground (z = 0), but the horizontal wind is undefined there. The lowest level at which it is defined is the first staggered level above the surface (at height $z = \Delta z/2$, where Δz is the vertical grid spacing

DOI: 10.1175/JAS-D-21-0020.1

next to the ground). This level is often referred to as the lowest scalar level. Consequently, there is uncertainty in the calculation of trajectories when they dip into the layer between the lowest scalar level and the ground (e.g., Dahl et al. 2014; Markowski and Richardson 2014). Often the horizontal wind \mathbf{v}_H is assumed unrealistically to be constant in this layer (e.g., Markowski and Richardson 2014), extrapolated from higher levels (Yokota et al. 2018; Tao and Tamura 2020), or, if the lower boundary condition is semislip, assumed to adhere to log-law behavior (e.g., Markowski 2016), which is probably unrealistic within convective storms (e.g., Markowski et al. 2019). The above problem with trajectories is also present in Doppler-radar analyses where there are no data between the lowest observation level and the ground (Markowski et al. 2012). Additional errors arise in circuit analyses because the forces influencing near-surface parcels (e.g., buoyancy) also have to be extrapolated from higher levels.

When interpreting the results of a circulation analysis, we should bear in mind that the circulation around a material circuit is unaffected by a vortex passing inside it (Fig. 1). In this context, Morton (1966, p. 182) stated that "It is interesting to note that there is some evidence for the existence around tornado cores of vorticity opposite in sense to that of the core (Hoecker 1960; Glaser 1960) so that the circulation around the core perimeter exceeds that in circuits of larger radius. If this is correct, it suggests that at least part of the air mass of the tornado column has been introduced from other presumably higher levels. (The circulation in a large circuit is unchanged when a funnel of rotating fluid dips down through it.)" Note that Morton's deduction is still valid if the rotating fluid passes through the circuit from below instead of from above. Although the material circuit will expand to accommodate the extra fluid (Fig. 1), the barotropic circulation around it will not react to a tornado developing upward or downward through it according to Kelvin's circulation theorem.

Sometimes it is useful to consider the circulation around a nonmaterial circuit. A point on such a circuit has a non-advective velocity, which is its velocity minus the wind at that point. For example, the nonadvective velocity of a point on a stationary curve is the negative of the wind at the point.

Computing the circulations around constrained curves that move partially with the wind and remain in the same plane can alleviate some of the aforementioned problems. With a horizontal circuit that moves with the horizontal wind \mathbf{v}_H , we can avoid the difficulty associated with parts of circuits dipping below the lowest scalar grid level. Another advantage is that the above fractal difficulty, if a problem, can be avoided easily in 2D by using Stokes's theorem to compute the circulation as an equivalent integral over a horizontal area. A disadvantage is that the circulation around horizontal curves is independent of horizontal vorticity so that this approach is oblivious to the "river-bend effect" wherein baroclinically or frictionally generated horizontal vorticity is reoriented from crosswise to streamwise. Note, however, that for a 3D material circuit the bend effect is hard to discern from the convoluted geometry of the circuit. As shown in section 4b, a circuit confined to a vertical plane is optimal for demonstrating the river-bend effect. Another disadvantage of analyses with level curves (i.e.,

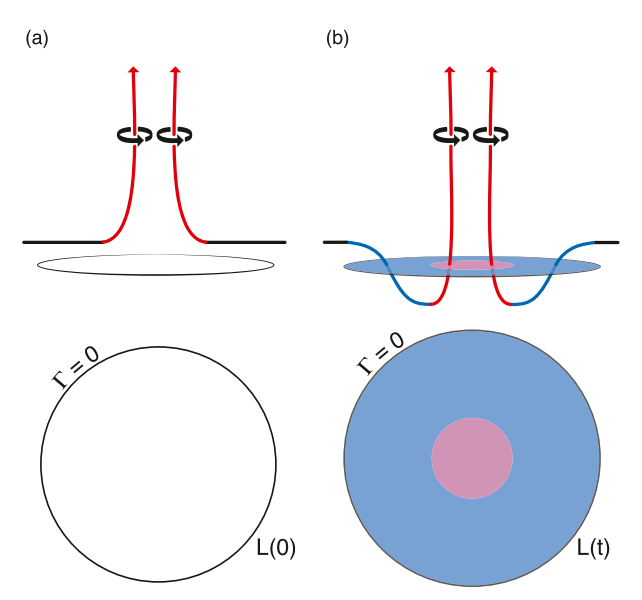


FIG. 1. Schematic showing vortex lines when a cyclonically rotating funnel of air dips down through a material circuit L that encloses an area A. In the 3D perspectives, the vortex line segments are colored red, black, or blue according to whether the vertical vorticity is cyclonic, zero, or anticyclonic, respectively. The curved arrows indicate the direction of rotation. In the horizontal sections, subareas of A where the vorticity is cyclonic or anticyclonic are shaded pink or blue, respectively. (a) At time zero, the funnel is above the initial circuit L(0), which has zero circulation. (b) At a later time t, the funnel has pierced the area A(t), which is now larger to accommodate the extra fluid. According to Kelvin's circulation theorem, there is still no circulation around L(t). For the areal average of vorticity normal to A to remain zero, the inner core of cyclonic vorticity within A(t) must be surrounded at least partly by a region of anticyclonic vorticity.

horizontal curves that stay at the same height) is that although tilting of horizontal vorticity into the vertical is included, it excludes baroclinic generation of horizontal vorticity, which is well represented in a 3D material circulation analysis prior to the circuit becoming flat. In a level-curve analysis, vertical forces are represented only through their accumulated effects on vertical velocity w. On the other hand, the rate of change of material circulation is independent of tilting and stretching, which have to be assessed from the complicated changing 3D configuration of a material circuit. Thus, the two analyses complement one another. Keeping the circuit level requires adding the circulation of the partial inertial force $-w\partial \mathbf{v}_H/\partial z$ to the circulation equation.

To determine the sensitivity of the circulation analyses to the size of the horizontal closed curve at the time t_1 , one could draw two circuits, one inside the other, and take both circuits backward to time t_0 . (This is not attempted in this paper.) If the closed curves are ones that move with the horizontal wind while staying in the same level, the smaller circuit is always contained inside the larger one. (If this were untrue, the curves would intersect at some time, which is impossible because intersection points move with the horizontal wind and thus remain on both curves for all time including t_1 .) If, on the other

hand, the detached curves are material ones that move in 3D, there is no containment and the only thing that can be said about how the two curves relate to each other is that they never intersect (because they do not share a common parcel). Thus, the configuration of the 3D curve at the earlier time t_0 may be very sensitive to the choice of the final curve at t_1 .

A hybrid approach can capture the best features of the 3D-and the flat-circuit circulation analyses. To circumvent the problem of a material curve passing below the lowest scalar level while retaining a 3D approach, we specify that the curve moves with the 3D flow everywhere above the height Δz . When a part of the material curve dips below this level, it is replaced with a horizontal curve segment that moves with the horizontal wind. We then make use of a generalized circulation theorem. The height $z = \Delta z$ is chosen because it is the lowest grid level at which the extra term is easily evaluated. Thus, the hybrid method still detects past baroclinic generation of circulation along elevated parts of the circuit while preventing the circuit from dipping into the layer of ill-defined wind next to the ground.

This paper is organized as follows. In section 2 and appendix A, we derive a general circulation theorem for a nonmaterial circuit. Section 3 adapts this theorem to special curves, and section 4 applies this theory to simple examples such as the linear theory of updraft rotation, flow around a bend, and axisymmetric flow. In section 5, we perform circulation analyses for a vortex that forms in a simulated supercell-like pseudostorm and compare the results for the horizontal circuit, the fully 3D circuit, and the hybrid circuit. Section 6 summarizes our main points.

2. A circulation theorem for a moving nonmaterial curve

We need a general circulation theorem for arbitrarily moving curves. Let t be time and $\mathbf{x} = x\mathbf{i} + y\mathbf{j} + z\mathbf{k}$ be the position vector, where \mathbf{i} , \mathbf{j} , and \mathbf{k} are eastward, northward, and upward unit vectors and z is height above (flat) ground. The presence or absence of a subscript a denotes an absolute or relative quantity, respectively. Davies-Jones (2004) derived the following theorem for the rate of change of the absolute circulation $\Gamma_a(t)$ around any simple closed oriented curve K(t) in a reference frame rotating with Earth:

$$\frac{\delta\Gamma_{a}}{\delta t} = \oint\limits_{K(t)} (\boldsymbol{\omega}_{a} \times \mathbf{N}) \cdot d\mathbf{x} - \oint\limits_{K(t)} \alpha \, dp - g \oint\limits_{K(t)} q_{l} \, dz + \oint\limits_{K(t)} \mathbf{F} \cdot d\mathbf{x}.$$
(1)

We derive this equation more rigorously than heretofore in appendix A. Thus, we can calculate the rate that circulation changes solely from quantities on the circuit itself regardless of values inside the circuit. The curve K can be stationary or moving in any specified way in two or three dimensions. In (1), \mathbf{N} is the nonadvective velocity of points on K(t), α is specific volume, p is pressure, g is the gravitational acceleration, q_l is the hydrometeor mixing ratio, and \mathbf{F} is the frictional force. On K, $\mathbf{N} \equiv \mathbf{V} - \mathbf{v}$ where $\mathbf{v} \equiv u\mathbf{i} + v\mathbf{j} + w\mathbf{k}$ is the wind vector and $\mathbf{V} \equiv U\mathbf{i} + V\mathbf{j} + W\mathbf{k}$ is the velocity of the curve points. On an f plane the absolute vorticity is

$$\boldsymbol{\omega}_{a} \equiv (\partial_{y} w - \partial_{z} v)\mathbf{i} + (\partial_{z} u - \partial_{y} w)\mathbf{j} + (\zeta + f)\mathbf{k}, \tag{2}$$

where $\partial_x \equiv \partial/\partial x$ and so on, $\zeta \equiv \partial_x v - \partial_y u$ is the relative vertical vorticity, and f is the Coriolis parameter. The general circulation equation in (1) states that the rate of change of absolute circulation is equal to the sum of the force circulations of the following forces per unit mass: pressure-gradient force, precipitation drag, and frictional force. There is also an additional term (the first one on the right side) that appears when the circuit is not a material one.

In the Boussinesq approximation ($\alpha = \alpha_0 + \alpha'$, $d\overline{p}/dz = -g/\alpha_0$, and $\alpha_0 = \text{constant}$), the second term on the right of (1) becomes

$$-\oint_{K(t)} \alpha \, dp \approx -\oint_{K(t)} \alpha' \frac{d\overline{p}}{dz} dz = \oint_{K(t)} \frac{g\alpha'}{\alpha_0} dz. \tag{3}$$

If we define the buoyancy force $B\mathbf{k}$ as $g(\alpha'/\alpha_0 - q_l)\mathbf{k}$, then the Boussinesq version of (1) is

$$\frac{\delta\Gamma_a}{\delta t} = \oint\limits_{K(t)} (\boldsymbol{\omega}_a \times \mathbf{N}) \cdot d\mathbf{x} + \oint\limits_{K(t)} B \, dz + \oint\limits_{K(t)} \mathbf{F} \cdot d\mathbf{x}. \tag{4}$$

The last two terms in (4) are the buoyancy and frictional force circulations. They are equal to the work done by the buoyancy and frictional forces on a parcel that is moved instantaneously once around K(t) in the positive direction. [If K(0) is horizontal at a time t = 0, the counterclockwise direction around K(0) and the mapping from K(0) to K(t) define the positive direction around K(t).]

3. Special cases

We now adapt the circulation theorem in (1) to special circuits. These circuits are material circuits, denoted by M(t), stationary curves S, level curves L(t), stationary level curves SL, and hybrid circuits Y(t). Level circuits are defined as ones that reside in one horizontal plane.

a. Material circuits

For material circuits, N = 0, and (1) reduces to

$$\frac{\delta\Gamma_a}{\delta t} = -\oint_{M(t)} \alpha \, dp - g \oint_{M(t)} q_t \, dz + \oint_{M(t)} \mathbf{F} \cdot d\mathbf{x},\tag{5}$$

which is Bjerknes theorem with frictional force (Dutton 1986, p. 372) and precipitation drag. The rate of change of circulation around a material circuit is equal to the sum of the force circulations. The barotropic circulation is constant (Kelvin's circulation theorem).

b. Stationary circuits

For a stationary curve S, N = -v and (1) becomes

$$\frac{\partial \Gamma_a}{\partial t} = -\oint_S (\boldsymbol{\omega}_a \times \mathbf{v}) \cdot d\mathbf{x} - \oint_S \alpha \, dp - g \oint_S q_I \, dz + \oint_S \mathbf{F} \cdot d\mathbf{x}, \quad (6)$$

where $\omega_a \times v$ is the sum of the Lamb vector $\omega \times v$ and the Coriolis acceleration.

c. Level circuits

For a level curve L(t), we let $\mathbf{N} = \mathbf{P} - w\mathbf{k}$, where $-w\mathbf{k}$ is the vertical nonadvective velocity required to keep the circuit horizontal (dz = 0) and \mathbf{P} is the horizontal nonadvective velocity of the curve points. Then (1) turns into

$$\frac{\delta\Gamma_{a}}{\delta t} = \oint\limits_{L(t)} (\zeta + f) \mathbf{P} \cdot \mathbf{n} \, ds - \oint\limits_{L(t)} w \frac{\partial \mathbf{v}_{H}}{\partial z} \cdot d\mathbf{x} - \oint\limits_{L(t)} \alpha \, dp + \oint\limits_{L(t)} \mathbf{F}_{H} \cdot d\mathbf{x}$$
(7)

(Davies-Jones 2004), where subscript H denotes the horizontal component, $\mathbf{n} = \mathbf{i} dy/ds - \mathbf{j} dx/ds$ is the outward horizontal unit normal to L(t), and ds is the element of arclength in the counterclockwise direction along L(t). The second term on the right of (7) has an alternative form, namely,

$$-\oint_{L(t)} w \frac{\partial \mathbf{v}_{H}}{\partial z} \cdot d\mathbf{x} = \oint_{L(t)} \left[-w \left(\frac{\partial u}{\partial z} - \frac{\partial w}{\partial x} \right) dx + w \left(\frac{\partial w}{\partial y} - \frac{\partial v}{\partial z} \right) dy \right]$$
$$= \oint_{L(t)} w \boldsymbol{\omega}_{H} \cdot \mathbf{n} \, ds \,. \tag{8}$$

Here we have used the fact that the integral of an exact differential around a closed circuit is zero. Hence the second term on the right of (7) is the " ω flux term" in (4.4) of Trapp and Weisman (2003). We can also relate the ω flux term to terms in the vertical-vorticity equation. By Stokes's theorem,

$$-\oint_{L(t)} w \frac{\partial \mathbf{v}_{H}}{\partial z} \cdot d\mathbf{x} = -\iint_{A(t)} \mathbf{k} \cdot \nabla \times (w \partial_{z} \mathbf{v}_{H}) dx dy$$

$$= \iint_{A(t)} (-\partial_{x} w \partial_{z} v + \partial_{y} w \partial_{z} u - w \partial_{z} \zeta) dx dy, \qquad (9)$$

where A(t) is the horizontal area enclosed by L(t). Thus, the second term on the right of (7) represents the rate of change of circulation from tilting of horizontal vorticity and vertical advection of vertical vorticity within the circuit. The first term on the right of (7) accounts for the rate that circulation increases as a result of advection of vertical vorticity into the horizontal area bounded by a horizontal curve that is moving differently from the horizontal wind ($\mathbf{P} \neq \mathbf{0}$). The last two terms in (7) are the solenoidal- and frictional-force circulations, respectively. If we make the Boussinesq approximation and assume that $\mathbf{F}_H = \nu_e \nabla^2 \mathbf{v}_H$, where ν_e is a constant eddy viscosity, then (7) becomes

$$\frac{\delta\Gamma_{a}}{\delta t} = \oint_{L(t)} (\zeta + f) \mathbf{P} \cdot \mathbf{n} \, ds - \oint_{L(t)} w \partial_{z} \mathbf{v}_{H} \cdot d\mathbf{x} + \nu_{e} \oint_{L(t)} \nabla_{H} \zeta \cdot \mathbf{n} \, ds + \nu_{e} \oint_{L(t)} \partial_{zz} \mathbf{v}_{H} \cdot d\mathbf{x}, \tag{10}$$

where the last two terms represent horizontal diffusion of vertical vorticity into A(t) and vertical shear diffusing vertically to C(t). Note that in the Boussinesq approximation there are no

solenoids in a horizontal plane and therefore the $-\oint_{\alpha} dp$ term does not appear in (10).

To investigate the growth of circulation around updrafts, Davies-Jones (2004) set w = 0 at the updraft edge and **P** equal to the propagation velocity of the edge points. Here we are interested in how circulation develops around a level curve that eventually surrounds a maximum of vertical vorticity near the ground. In this situation, we retain the second term and in the first term set **P** = **0** for a level curve that moves with the horizontal wind (so that there is no horizontal flux into or out of the enclosed area).

d. Stationary level circuits

For a stationary level curve SL, we set $\mathbf{P} = -\mathbf{v}_H$ and $\mathbf{N} = -\mathbf{v}$. Then (7) becomes

$$\frac{\partial \Gamma_a}{\partial t} = \oint_{SL} (-\zeta \mathbf{v}_H - f \mathbf{v}_H + w \boldsymbol{\omega}_H) \cdot \mathbf{n} \, ds - \oint_{SL} \alpha \, dp + \oint_{SL} \mathbf{F}_H \cdot d\mathbf{x}$$
(11)

after use of (8). In the Boussinesq approximation, the solenoidal term vanishes and this equation becomes equivalent to (4.4) in Trapp and Weisman (2003).

e. Hybrid circuits

For the hybrid circuit with its flat base at $z = \Delta z$, $\mathbf{P} = \mathbf{0}$ at all points, and $\mathbf{N} = \mathbf{0}$ at all heights greater than Δz . If w < 0 at the level $z = \Delta z$, then $\mathbf{N} = -w\mathbf{k}$ there so that the curve points never dip below this level. Let $\mu = 1$ on the horizontal floor of the curve and 0 otherwise. From (1), the rate that circulation around the hybrid circuit changes is

$$\frac{\delta\Gamma_{a}}{\delta t} = -\oint_{Y(t)} \mu w \frac{\partial \mathbf{v}_{H}}{\partial z} \cdot d\mathbf{x} - \oint_{Y(t)} \alpha \, dp - g \oint_{Y(t)} q_{l} \, dz + \oint_{Y(t)} \mathbf{F} \cdot d\mathbf{x}.$$
(12)

Relative to (5) for a totally material curve, (12) has an extra term, the first one on the right. This is the ω flux term. It applies here only to the horizontal floor of the circuit. Since w < 0 on the floor, the term contributes positively to the rate of change of circulation where the vertical shear vector is directed along the curve in the positive direction. Alternatively, via (8), horizontal vorticity vectors aligned with the inward normal to the circuit act to increase the circulation [as in Fig. 10 of Trapp and Weisman (2003)].

4. Examples

The following examples illustrate how use of the generalized circulation theorem in (1) with a nonmaterial circuit instead of a material one simplifies explanation of several supercell phenomena. Since the planetary vorticity is small relative to the horizontal vorticity in the environment (Davies-Jones 1984), we henceforth neglect the planetary vorticity, as is customary in supercell dynamics.

a. Linear theory of updraft rotation

We start by using the circulation theorem to prove a well-known result. Davies-Jones (1984) used linear theory to show

that an updraft with a circular cross section rotates cyclonically as a whole when the vorticity in the environment is streamwise to the storm-relative wind $\overline{\mathbf{v}}(z) - \mathbf{c}$. Here \mathbf{c} is the storm-motion vector, and the overbar denotes environmental quantity. The environmental shear vector $\overline{\mathbf{S}}(z)$ is then 90° to the right of the relative environmental wind. In inviscid linear theory, we may let the level curve L(t) be a circle at height h that moves centrally through the updraft from far upstream with the constant velocity $\overline{\mathbf{v}}(h) - \mathbf{c}$. Then $\mathbf{P} = \mathbf{0}$, and in the absence of torques (7) reduces to

$$\frac{\delta\Gamma}{\delta t} = -\oint_{L(t)} w\overline{\mathbf{S}} \cdot d\mathbf{x}, \qquad (13)$$

where the positive direction around L(t) is counterclockwise. The circulation Γ is zero upstream. The circle acquires circulation as its leading edge moves into the updraft because w>0 and $-\overline{\mathbf{S}}\cdot d\mathbf{x}>0>0$ at the leading edge, with w=0 still at the trailing edge (Fig. 2). Conversely, the circle loses circulation as it exist he updraft (now w=0 at the leading edge; w>0 and $-\overline{\mathbf{S}}\cdot d\mathbf{x}<0$ at the trailing edge) until its circulation returns to zero after it has completely passed through the updraft. Inside the updraft, the circulation is positive (cyclonic) as Lilly (1982) and Davies-Jones (1984, 2004) concluded by different means. Since the environmental vorticity $\overline{\boldsymbol{\omega}} = \mathbf{k} \times \overline{\mathbf{S}}$, an alternative version of (13) is

$$\frac{\delta\Gamma}{\delta t} = \oint_{L(t)} w\overline{\boldsymbol{\omega}} \cdot \mathbf{n} \, ds. \tag{14}$$

Thus, the right side of (13) is the linearized version of the ω flux term on the right side of (8).

The important component of nonadvective velocity in this example is the vertical one, which cancels the updraft's vertical velocity and keeps the circuit in its horizontal plane. To explain updraft rotation using a material circuit would entail the complicated process of drawing a horizontal curve around the updraft, taking the curve to earlier times using backward trajectories, and seeing how the environmental vortex lines threaded the deformed circuit.

b. Flow around a bend

To illustrate the development of streamwise vorticity around a left-hand bend (Fig. 3), we use a planar vertical circuit, which revolves around the bend's center of curvature as a solid body. The normal to the plane is in the direction of the primary flow and perpendicular to the radius vector from the center of curvature. Because of surface friction, the flow entering the bend is vertically sheared with the flow speed being an increasing function of z and the primary vorticity ω_0 being directed leftward of the flow. The vertical vorticity ζ of each parcel is zero upstream and is conserved approximately (Shapiro 1972) as there is practically no torque about a vertical axis. Therefore, the shear vorticity cancels curvature vorticity, and the flow is faster on the inside of the bend and slower on the outside of the bend. The flow would swivel a material circuit about a vertical axis and tilt it downshear. Hence the nonadvective velocity N required to

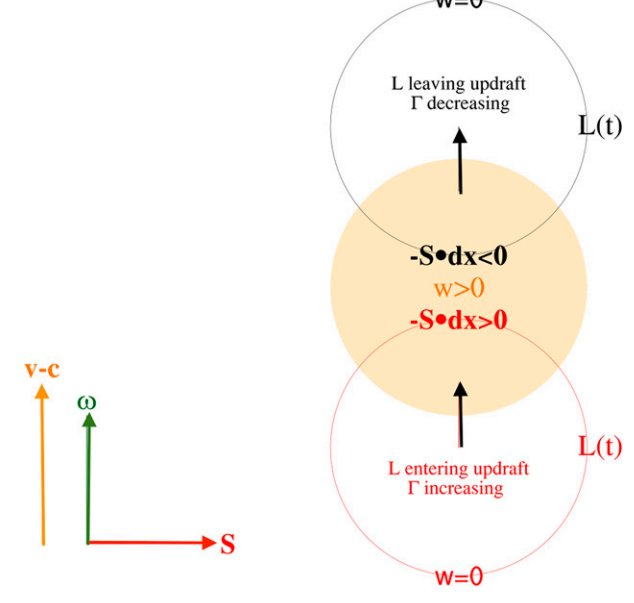


FIG. 2. Linear theory of overall updraft rotation (or of positive circulation around the updraft). Green and red arrows depict the environmental vorticity vector and shear vector \overline{S} , respectively. The circle L(t) moves with the environmental storm-relative wind (orange arrow) centrally through the updraft (shaded orange). Note that the storm-relative environmental vorticity is streamwise. The positive direction around L is counterclockwise. As L enters the updraft (w > 0) the circulation around L increases from zero as a result of positive $\oint (-w)\overline{\mathbf{S}} \cdot d\mathbf{x}$ or equivalently positive $\oint w\overline{\omega} \cdot \mathbf{n} \, ds$, where \mathbf{n} is the outward normal to L. When L is concentric with the updraft, the circulation around L reaches its maximum value, which is equal to that of the updraft. Thereafter, $\oint (-w)\overline{\mathbf{S}} \cdot d\mathbf{x}$ and $\oint w\overline{\omega} \cdot \mathbf{n} \, ds$ turn negative, and the circulation around L decreases, becoming zero again when L is completely outside the updraft.

keep the circuit in solid-body rotation consists of N_1 , which is upstream on the inside of the bend and downstream on the outside of the bend, and N_0 , which is upstream in the upper part of the flow and downstream in the lower part of the flow (Fig. 3). To a first approximation,

$$\mathbf{N} \approx \mathbf{N}_0(z) + \mathbf{N}_1(r) = -v_0(z)\mathbf{t} - v_1(r)\mathbf{t}$$
 (15)

in cylindrical coordinates, where r is distance from the axis (center of curvature), \mathbf{t} is the unit downstream vector, $v_0(z)$ is the primary flow, and $v_1(r)$ is the adjustment in the downstream wind component required for ζ to remain zero. The primary vorticity is

$$\boldsymbol{\omega}_0 = \frac{dv_0}{dz}\mathbf{n},\tag{16}$$

where \mathbf{n} is the unit vector to the left of the flow. Hence,

$$\boldsymbol{\omega}_0 \times \mathbf{N} \approx \frac{d}{dz} \left(\frac{v_0^2}{2}\right) \mathbf{k} + \frac{dv_0}{dz} v_1(r) \mathbf{k}.$$
 (17)

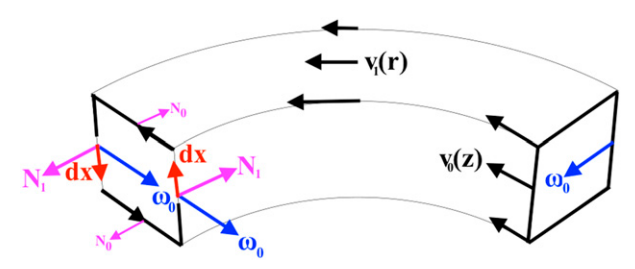


FIG. 3. Three-dimensional diagram of streamwise-vorticity development around a left-hand bend (thin black lines). Black arrows on the inner bank of the bend entrance indicate the vertical profile $\mathbf{v}_0(z)$ of the primary downstream flow. Black arrows on the top face at top midbend show the lateral profile $\mathbf{v}_1(r)$ of downstream velocity that develops in the bend. The vertical circuit (thick black lines) revolves around the bend's center of curvature as a solid body. The blue arrows indicate the direction of the primary transverse vorticity $\boldsymbol{\omega}_0$. The magenta arrows depict the non-advective velocity $\mathbf{N} (= \mathbf{N}_0 + \mathbf{N}_1)$ required to keep the circuit in solid-body rotation, and the red arrows show the direction of $d\mathbf{x}$ around the circuit. The black transverse arrows at the exit of the bend indicate the sense of the secondary streamwise circulation produced by the positive $\boldsymbol{\omega}_0 \times \mathbf{N} \cdot d\mathbf{x}$.

If we assume that the frictional term is small, then the rate of circulation change is

$$\frac{\delta\Gamma}{\delta t} \approx \oint_{K(t)} \left[\frac{d}{dz} \left(\frac{v_0^2}{2} \right) \mathbf{k} + \frac{dv_0}{dz} v_1(r) \mathbf{k} \right] dz = \oint_{K(t)} \frac{dv_0}{dz} v_1(r) dz \quad (18)$$

from (4) and (17). The direction of $d\mathbf{x}$ around the circuit is given by the right-hand rule with the thumb pointing downstream. Hence, at the inside of the bend dz is positive and u(r) is greatest and at the outside of the bend dz is negative and u(r) is least. Thus $\delta\Gamma/\delta t > 0$, indicating generation of secondary streamwise circulation in the bend.

c. Vortex formation in axisymmetric flow

In axisymmetric simulations of tornadogenesis (e.g., Markowski et al. 2003; Davies-Jones 2008), L(t) would be a horizontal circle of variable radius $\sigma(t)$ centered on the axis. In this section, M represents angular momentum. The circulation Γ is related to M by $\Gamma \equiv 2\pi M$. In cylindrical coordinates (r, ϕ, z) with corresponding wind components $(u_r, M/r, w)$, imposing axisymmetry on (7) yields the angular-momentum equation

$$\frac{\delta M}{\delta t} = -w\partial_z M|_{r=\sigma} - \lambda (u_r \partial_r M)|_{r=\sigma} + \nu_e \left[\partial_{zz} M + r\partial_r \left(\frac{1}{r} \partial_r M \right) \right] \Big|_{r=\sigma}$$
(19)

where we have assumed for simplicity a constant eddy viscosity ν_e . Here $\lambda=1$ for a stationary circle and $\lambda=0$ for a circle that moves horizontally with the radial wind u_r so that there is no horizontal influx of angular momentum into the circle of radius σ . The solenoidal torque does not appear in (19) because of the axisymmetry.

For the Rott (1958) vortex [see also Davies-Jones and Wood (2006)], *M* increases radially outward (assuming a cyclonic

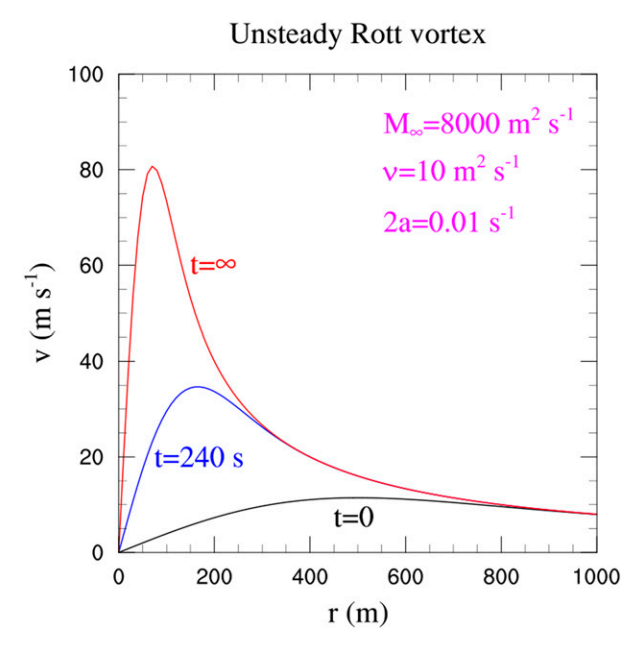


FIG. 4. Radial profiles of tangential wind v(r, t) for the Rott convergent vortex at three different times. The parameters M_{∞} , ν , and 2a are the angular momentum at radial infinity, constant eddy viscosity, and constant horizontal convergence, respectively. At the arbitrary initial time t=0, the radius of maximum tangential wind is 500 m. The tangential wind approaches the steady state ($t=\infty$) asymptotically.

vortex in the Northern Hemisphere) and is independent of height. In this case (19) reduces to

$$\frac{\delta M}{\delta t} = -\lambda (u_r \partial_r M)|_{r=\sigma} + \nu_e \left[r \partial_r \left(\frac{1}{r} \partial_r M \right) \right] \Big|_{r=\sigma}. \tag{20}$$

An initially wide Rott vortex contracts in convergent flow $(u_r = -ar, w = 2az, \text{ and } a = \text{const} > 0)$ until inward advection of M is balanced by outward diffusion of M (Fig. 4). From the perspective of (20) with $\lambda = 1$, M at a fixed radius r^* changes at a rate equal to its inward advection minus its outward diffusion. For $\lambda = 0$, the circle contracts asymptotically to the axis. As it does so, the circulation around it decreases owing to outward diffusion of M.

We now examine a more general case in which M varies with height. The Davies-Jones (2008) axisymmetric model shows how rotation develops next to the ground in a flow initially devoid of low-level rotation and how a tornado can form according to Fujita's (1973) recycling hypothesis. The domain of radius R is closed with no-slip boundary conditions imposed on the tangential wind and free-slip on the other wall-parallel components. The initial condition is an updraft that is rotating at midlevels surrounded by a compensating downdraft (Fig. 5). In axisymmetric flow the angular-momentum contours are also the vortex lines. Precipitation drag initiates a downdraft around the periphery of the updraft. This downdraft and its outflow transports air with significant angular momentum downward and inwards, thereby increasing the circulation at (r, z) = (0.25, 0.1), for example (Fig. 6). Near the axis, this air is

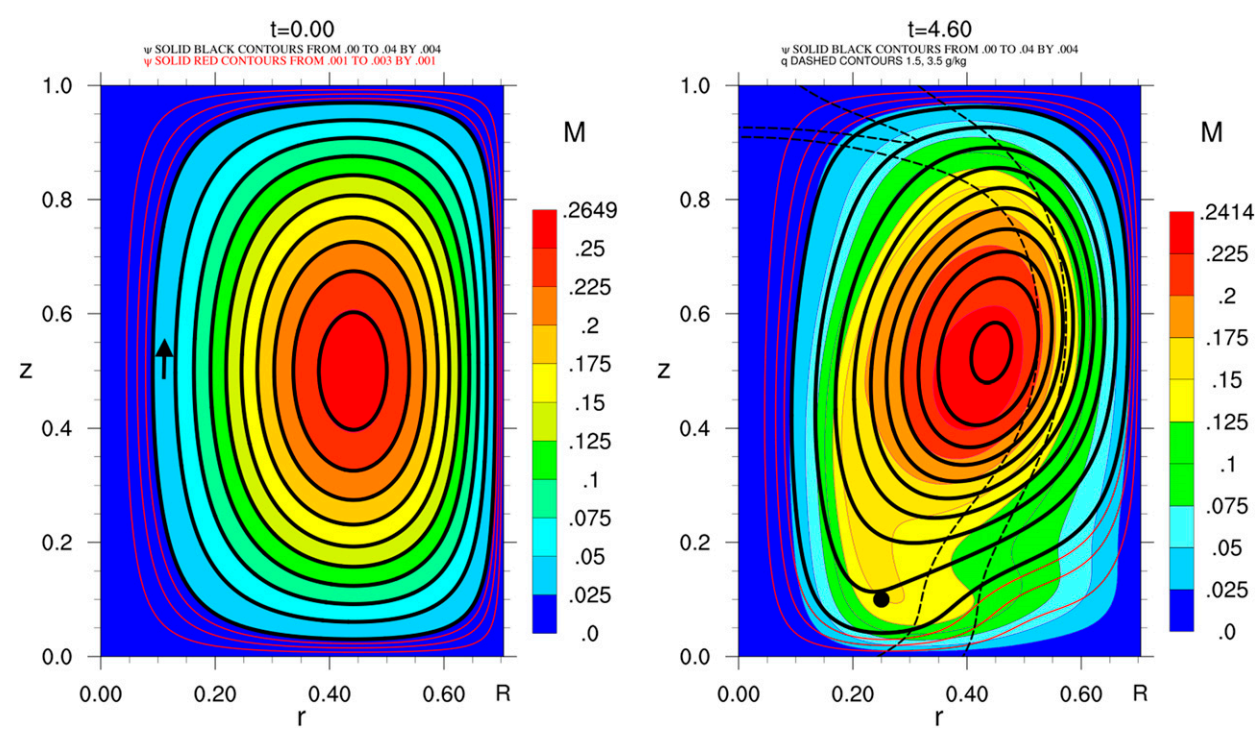


FIG. 5. Initial fields of angular momentum M (color-shaded contours) and streamfunction ψ (red and black solid-line contours) in the Davies-Jones (2008) main experiment. The arrow shows flow direction in the radial-height plane. The contours of M are also the vortex lines.

FIG. 6. As in Fig. 5, but at a later time t = 4.6. The dashed contours are for rain mixing ratio. The black dot indicates a location at which the circulation is increasing as a result of downward angular momentum advection.

drawn into the updraft. From loss of angular momentum to the ground, air that flows next to the surface penetrates close to the axis before rising and abruptly spreading out. In Fig. 7a tornado is present. The tornado forms from the ground up with the circulation in the tornado at (0.08, 0.1) increasing as a result of upward advection.

The domain's bounding surface is a material surface with zero angular momentum. This statement is true either by virtue of the boundary conditions when the fluid is viscous or by virtue of the initial condition and conservation of angular momentum when the fluid is inviscid. Now consider the circulation around concentric horizontal circles of radius σ in a given level (say z=0.1 in Fig. 5). When $\sigma=R$ the circle is also a stationary material circle and always has zero circulation regardless of rotating air dipping through it. It is therefore an example of Morton's deduction (see section 1) but with the rotating fluid building upward instead of dipping downward. The areal mean vertical vorticity in the disk enclosed by this circle is zero. The precipitation-induced downdraft has dragged down vortex lines, which reascend close to the axis. Thus, the cyclonic tornado is surrounded by anticyclonic vorticity.

In the numerical experiment, diffusion is a slow process relative to advection. From (19) the circulation around a smaller stationary circle $\sigma < R$ therefore increases if there is either a horizontal flux of angular momentum into the circle or vertical advection of angular momentum on the circle or both. For a circle of radius $\sigma(t)$ that moves in its horizontal plane with

the radial wind, the horizontal flux vanishes and circulation increases when there is positive vertical advection of M at the circle circumference. Consider such a circle inside of the rain curtain at a low height. As it contracts in the converging flow, its circulation increases at first owing to angular momentum bring transported downward from above and later owing to angular momentum bring transported upward from below, as indicated at the black dots in Figs. 6 and 7. In both situations, $-w\partial_z M$ at $r = \sigma(t)$ is positive. According to this experiment, observations (Fujita 1973), and numerical simulations (e.g., Markowski and Richardson 2014), it seems that all of the air in a tornado has descended at some distance from the axis of rotation before ascending in the core. The tornado vortex develops upward (Davies-Jones 2008), as has been recently observed with mobile Doppler radar by Bluestein et al. (2019).

5. Circulation analyses of a simulated supercell-like pseudostorm

To test the benefits of using horizontal or hybrid circuits as compared with fully 3D ones in the general circulation theorem in (1), we performed some circulation diagnostics of the CM1 model Sc8m8 simulation of Markowski and Richardson (2014). This is their main simulation, the one that produces a long-lived tornado-like vortex (TLV). A specified stationary heat source is activated in an environment with a semicircular hodograph of radius 8 m s⁻¹. The environmental shear is greatest

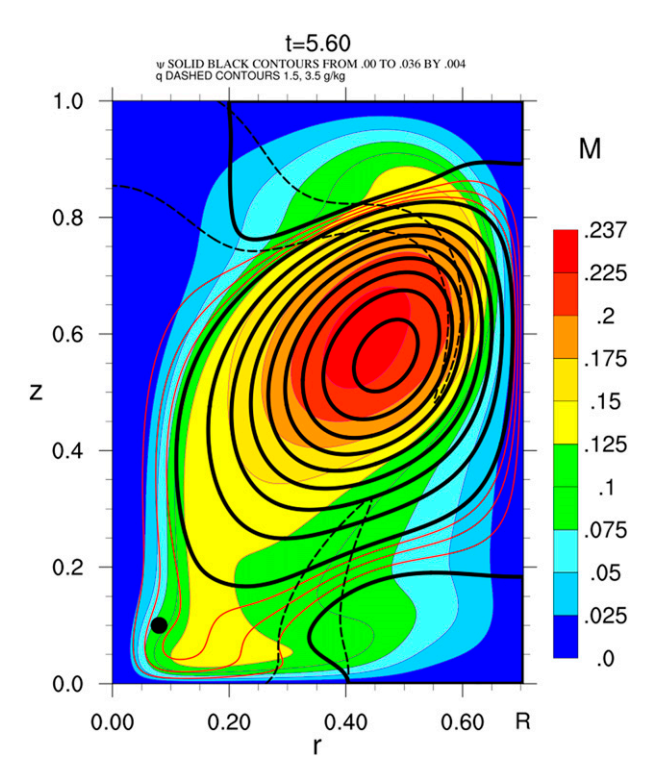


FIG. 7. As in Fig. 6, but at time t = 5.6. The black dot illustrates a region in the tornado where the circulation is increasing as a result of upward angular momentum advection. As evidenced by the vortex lines, the intensifying cyclonic vortex is surrounded by a wide region of anticyclonic vorticity.

in the lowest 1 km and decreases rapidly with height. The lower boundary condition is w = 0 at z = 0 and is "free slip" (i.e., no variation in the shear stresses τ_{13} and τ_{23} between z = 0 and z = Δz). After 15 min a quasi-steady rotating updraft has formed, at which time a low-level stationary heat sink close to the north-northeast of the heat source is activated. TLV formation is at t = 46 min, hereinafter t - 0. The grid spacing is 100 m in x, y, and z within the lowest 1 km of the central $20 \,\mathrm{km} \times 20 \,\mathrm{km}$ region of the domain. Horizontal grid stretching is used outside that region. Throughout the domain, the lowest level for u and v in the staggered grid is 50 m; thus, z = 100 m represents the first level at which centered finite differences can evaluate $w\partial_z \mathbf{v}_H$ and horizontal vorticity (from the horizontal winds at $z = 50 \,\mathrm{m}$ and $z = 150 \,\mathrm{m}$, and the vertical wind at $100 \,\mathrm{m}$). The circuits at t-0 are horizontal circles of radius 1 km surrounding the vortex at a height of 100 m AGL. A radius of 1 km is sufficiently large to mostly avoid problems arising from tracking the circuits backward in time through large velocity gradients associated with the vortex. The circuits are traced backward in time using the specified velocities of the curve points. As in Markowski and Richardson (2014), we use a fourth-order Runge-Kutta scheme to compute backward trajectories. The trajectory time step is -1 s, and the model output is saved every 5 s. (Saving the model output every second and using a trajectory time step of -0.25 s led to negligible changes in the circulation budgets.) Second-order extrapolation is used to assign values of a scalar s(x, y, z) such as a horizontal wind component, a momentum forcing, or temperature, to parcels that pass below the lowest scalar level. At fixed x and y, let s = f(z). We extrapolate f below $z = 0.5\Delta z$ by using the quadratic polynomial that passes through the three points $[0.5\Delta z, f(0.5\Delta z)], [1.5\Delta z, f(1.5\Delta z)],$ and $[2.5\Delta z, f(2.5\Delta z)]$. For this case, the Lagrange interpolating formula yields $f(z) = 0.5\varepsilon(\varepsilon - 1)f(0.5\Delta z) + (1 - \varepsilon^2)f(1.5\Delta z) + 0.5\varepsilon(\varepsilon + 1)$ $f(2.5\Delta z)$, where $\varepsilon = (z - 1.5\Delta z)/\Delta z$.

The maximum spacing allowed between adjacent parcels in the circuits as they are run backward in time is 10 m. When the spacing exceeds this limit, new parcels are added to the circuit via interpolation.

The configurations of the 3D, hybrid, and horizontal circuits at various times are shown in Fig. 8. The hybrid circuit has a floor at $z = \Delta z = 100 \,\mathrm{m}$ AGL, below which the circuit is not allowed to dip. At the time t - 0, the 3D-material, the hybrid, and the horizontal circuits are coincident and lie in the floor. Each parcel on the 3D circuit is associated with curve points on the hybrid and horizontal circuits, the ones that are collocated with it at t - 0. Curve points on the horizontal circuit are constrained to move just with the horizontal wind. Thus, the 3D circuit separates from the horizontal one when its parcels have nonzero vertical velocity. Curve points on the hybrid circuit also move with the horizontal wind, but with the vertical wind too when they are not constrained to the floor. Because the trajectories are backward ones, a parcel continuously in downdraft stays above the floor and remains coincident with its associated hybrid-curve point. Conversely, hybrid-curve points that are held to the floor are in regions where the near-ground vertical wind is upward. As a parcel first dips below the floor along its 3D backward trajectory, its associated hybrid-curve point follows a different path along the floor. The two circuits thus split apart. Since the flow is mostly divergent in reverse time, all the circuits become widely separated as they are traced backward in time.

The horizontal circuit is much shorter and less convoluted in backward time than the 3D and hybrid circuits. At $t-30\,\mathrm{min}$, the 3D and hybrid circuits require $\sim 750\,000\,\mathrm{parcels}$ to maintain a spacing of less than 10 m between adjacent parcels. In contrast the 2D horizontal circuit only requires $\sim 25\,000\,\mathrm{parcels}$. At least some of the "folds" in the circuits are the result of adjacent circuit parcels being "captured" within the vortex for different numbers of orbits before "escaping" in backward time. Such parcels become widely separated quickly.

In considering the circulations and their budgets for the different curves as functions of time (Fig. 9), we should remember that the curves and the circulations around them are the same only at the final time t-0 and that the only material circuit is the 3D one. For the other two circuits, Kelvin's theorem for barotropic circulation does not apply. Note that the subgrid-scale turbulence scheme's contribution to \mathbf{F} is relatively small in these simulations and therefore the frictional force \mathbf{F} is dominated by numerical diffusion. The advection scheme is odd ordered, and such schemes have implicit diffusion. Thus, additional explicit diffusion is not used, in accordance with the "industry standard" these days. The implicit-diffusion effects on velocity tendencies are diagnosed

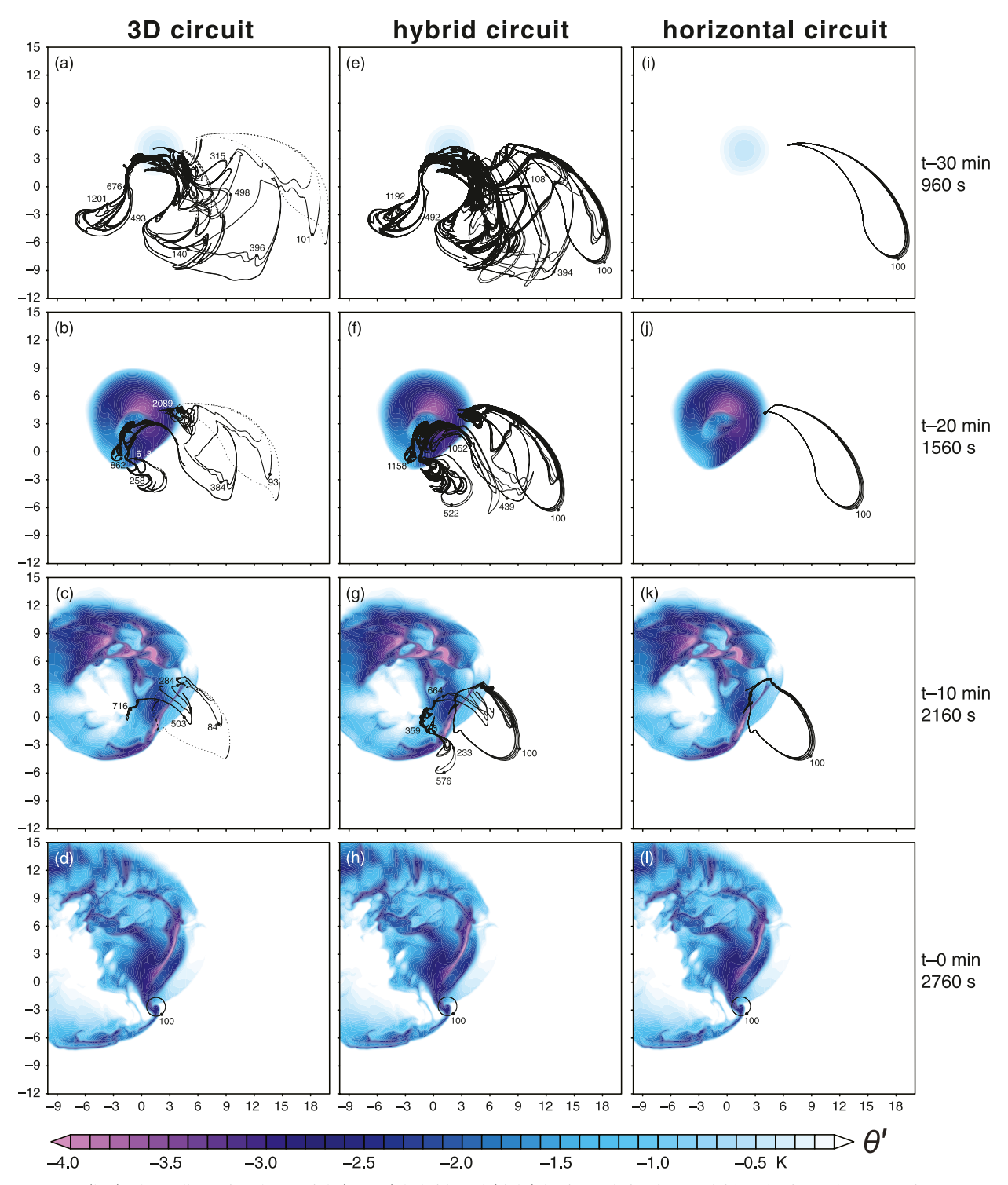


FIG. 8. (left) Three-dimensional material, (center) hybrid, and (right) horizontal circuits overlaid on horizontal cross sections of potential temperature perturbation (color shades) at z = 50 m in the Markowski and Richardson (2014) Sc8m8 simulation of a supercell-like pseudostorm at (a) 16 min or t = 30 min, (b) 26 min or t = 20 min, (c) 36 min or t = 10 min, and (d) 46 min or t = 0 min, the time of maximum cyclonic vorticity at the lowest model level. The altitudes of the circuits above the surface are indicated in meters at select locations, and a dotted curve is used where the circuit dips below the lowest model level for horizontal wind. Axis labels are distances in kilometers.

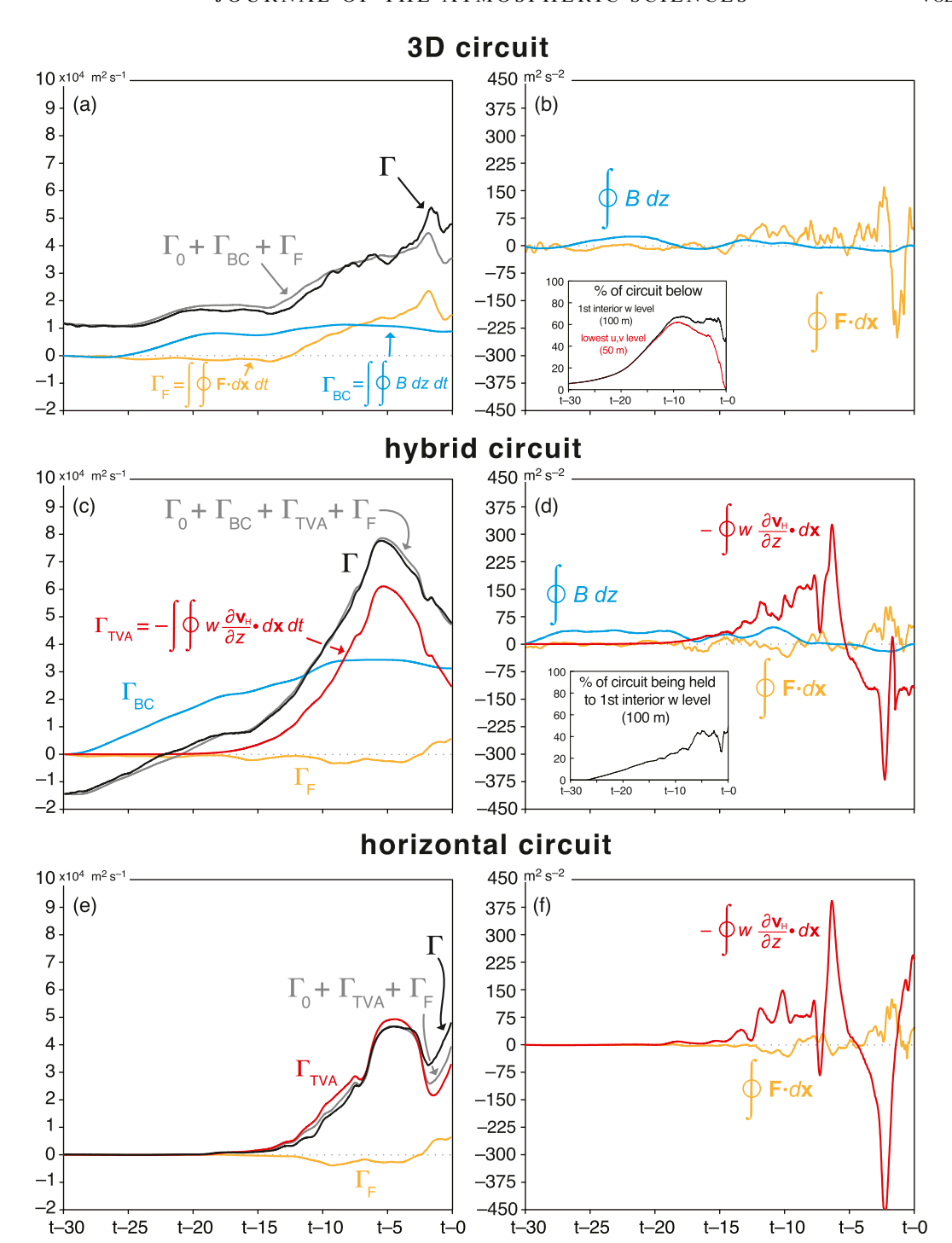


Fig. 9. Circulations, partial circulations, and force circulations about the (top) three-dimensional, (middle) hybrid, and (bottom) horizontal circuits, respectively, analyzed in the Markowski and Richardson (2014) Sc8m8 simulation of a supercell-like pseudostorm as functions of time. The time labels are as in Fig. 8. (a),(c),(e) Circulations and partial circulations about the three-dimensional, hybrid, and horizontal circuits, respectively. (b),(d),(f) Contributions to circulation tendencies from baroclinity, tilting and vertical advection (the ω flux term), and viscous effects (turbulent plus numerical diffusion). The inset in (b) shows the percentages of the 3D circuit that are below 100 m (black curve) and below the lowest scalar level at z = 50 m (red curve) as functions of time. The inset in (d) gives the percentage of the hybrid circuit that is being held to the first interior level for vertical shear and vertical velocity (z = 100 m). At t = 0 all parcels are at 100 m AGL.

at runtime and written to output. These diagnostics are probably less than perfect, even away from the ground, in regions of large velocity gradients.

We now compare the results of the circulation analyses for the different circuits. At t-0, Γ is about $5\times 10^4\,\mathrm{m}^2\,\mathrm{s}^{-1}$, which is a typical circulation for a strong tornado. Using the time integral of (12) from $t-30\,\mathrm{min}$ to t, we partition the total circulation Γ around each circuit into partial circulations Γ_0 , Γ_{BC} , Γ_{TVA} , and Γ_F , where Γ_0 is the circulation at $t-30\,\mathrm{min}$ (practically the initial circulation), Γ_{BC} is the baroclinic circulation or the buoyancy-force circulation, Γ_{TVA} is the circulation due to tilting of horizontal vorticity and vertical advection of vertical vorticity into the area A(t) bounded by K(t), and Γ_F is the diffusive circulation (the time integral of the frictional-force circulation). Alternatively, Γ_{TVA} is the integral over time of the circulation of the force needed to keep horizontal segments of the circuit level.

There is almost no circulation around the horizontal circuit at 100 m AGL 15 min prior to vortex formation (Figs. 9e,f). Since the circuit is horizontal, the buoyancy force cannot generate circulation around it. Thus Γ_0 and $\Gamma_{\rm BC}$ are both zero. The growth in circulation between t-15 and t-5 min is due entirely to $\Gamma_{\rm TVA}$ because Γ_F in this time interval is slightly negative. Note, however, that frictional or baroclinic torques near the ground may have generated some of the horizontal vorticity that is tilted into A(t).

For the 3D material circuit (Figs. 9a,b), the circulation Γ_0 at t-30 min is about $1\times 10^4\,\mathrm{m}^2\,\mathrm{s}^{-1}$. Since the rate of change of circulation from torques at early times is negligible, Γ_0 in this case is nearly the barotropic circulation, which is conserved since the circuit is a material one (Kelvin's circulation theorem). For a material circuit, Γ_{TVA} is zero and effects of tilting and stretching are concealed in the changing 3D geometry of the circuit. Initial circulation increase is due to Γ_{BC} , but this source of growth fades as the circuit levels out. For the last 12 min before vortex formation, the circulation intensifies because of Γ_F , which exceeds Γ_{BC} in the last 7 min. The sum of Γ_0 , Γ_{BC} , and Γ_F is less than Γ at t-0. This suggests that Γ_F , which is less accurately estimated than Γ_{BC} , may be underestimated at the time that the vortex forms.

The hybrid circuit has the largest change in Γ between t-30 and t-0 min (Figs. 9c,d). In this interval, the diffusive circulation Γ_F is small. From a negative initial value, the circulation increases initially because of $\Gamma_{\rm BC}$; $\Gamma_{\rm TVA}$ supplies the circulation spurt between t-12 and t-5 min as the circuit levels out and $\Gamma_{\rm BC}$ stops increasing.

Like the blind men and the elephant, the circulation analyses detect different features but not the entirety. The horizontal circuit sees the development of vertical vorticity in the last 15 min prior to TLV formation. Its circulation is due to vertical advection of vertical vorticity and tilting of horizontal vorticity toward the vertical into the area enclosed by the circuit. Amplification of vertical vorticity is implicit in the circuit's contraction. Circulation around the 3D material circuit increases as a result of buoyancy-force circulation in the interval from t-20 to t-15 min (but none later because of the circuit becoming flat) and to frictional-force circulation in the last 10 min prior to the tornado. From this perspective,

the frictional circulation becomes the dominant partial circulation. The effects of vorticity advection, tilting, and stretching are all implicit in the circuit's changing geometry. The hybrid circuit reacts chiefly to baroclinic generation of vorticity in the interval from t-25 to t-10 min and to tilting of horizontal vorticity toward the vertical and vertical advection of vertical vorticity during the last 12 min prior to the tornado. For the hybrid circuit, the frictional circulation is insignificant. The baroclinic circulations for the hybrid and 3D circuits are different (Fig. 9) because the circuits are different at all elevations.

The circulation imbalance $\Gamma - (\Gamma_0 + \Gamma_{BC} + \Gamma_{TVA} + \Gamma_F)$, which ideally should vanish, is much lower for the hybrid circuit than for the other two circuits for two reasons. First, the hybrid circuit has none of its points below 100 m whereas the 3D circuit has a high percentage of its points in the lowest 50 m (Fig. 9b) where the horizontal wind is ill defined. Second, given that the hybrid circuit obtains at least part of its circulation from the baroclinic forcing, which varies far more smoothly than the circulations of \mathbf{F} and $-w\partial_z(\mathbf{v}_H)$ (Fig. 9), the hybrid circuit's circulation budget is more accurate than that of the horizontal circuit, which depends solely on \mathbf{F} and $-w\partial_z(\mathbf{v}_H)$, both of which are more error prone than B. We also conducted circulation analyses (not shown) for circuits at 250 m AGL at t-0. The hybrid circuit again had the least circulation imbalance.

Heat maps of normalized baroclinic and viscous circulation forcing $(Bdz/|d\mathbf{x}|)$ and $\mathbf{F} \cdot d\mathbf{x}/|d\mathbf{x}|$, respectively) are provided in Fig. 10 to show the vertical extent of the circuits and how the circulation forcings are distributed in time and height. Tao and Tamura (2020, their Fig. 11b) showed a similar heat map for frictional forcing in their case study. Given how convoluted the circuits are, we found it futile to use a scheme as in Roberts and Xue (2017, their Fig. 8) by which the circuits shown in Fig. 8 are colored in proportion to the circulation forcings. The significant positive Γ_F acquired by the 3D circuit (Fig. 9a), which is perhaps surprising, is mainly the result of positive circulation forcing from turbulent and numerical diffusion along portions of the circuit that have dipped below the lowest scalar level (50 m) (Fig. 10b, inset). Given that these forcings have been extrapolated, it would be prudent to view them with skepticism. There are other reasons to be cautious about conclusions drawn from partitioning the circulation forcings into parts along segments. First, the quantities $Bdz/|d\mathbf{x}|$ and $\mathbf{F} \cdot d\mathbf{x}/|d\mathbf{x}|$ are the integrands. The line integrals themselves are the result of integrating these quantities with respect to a material arclength that is generally decreasing with (forward) time. The arclength factor is unrepresented in the heat maps. Second, as revealed by the derivation in appendix B, the rate of change of the line integral of wind along each material segment of the circuit contains an extra term (which vanishes around a closed curve) in addition to the line integrals of the buoyancy and frictional forces. For an asymmetric vortex this extra term could be significant (appendix B) and should not be ignored. For a steady axisymmetric tornado (e.g., Figs. 5-7), the frictional-force circulation near the ground should reduce circulation around an axisymmetric circuit so that inflowing parcels approach the axis more closely and rotate faster (Fiedler and Rotunno 1986;

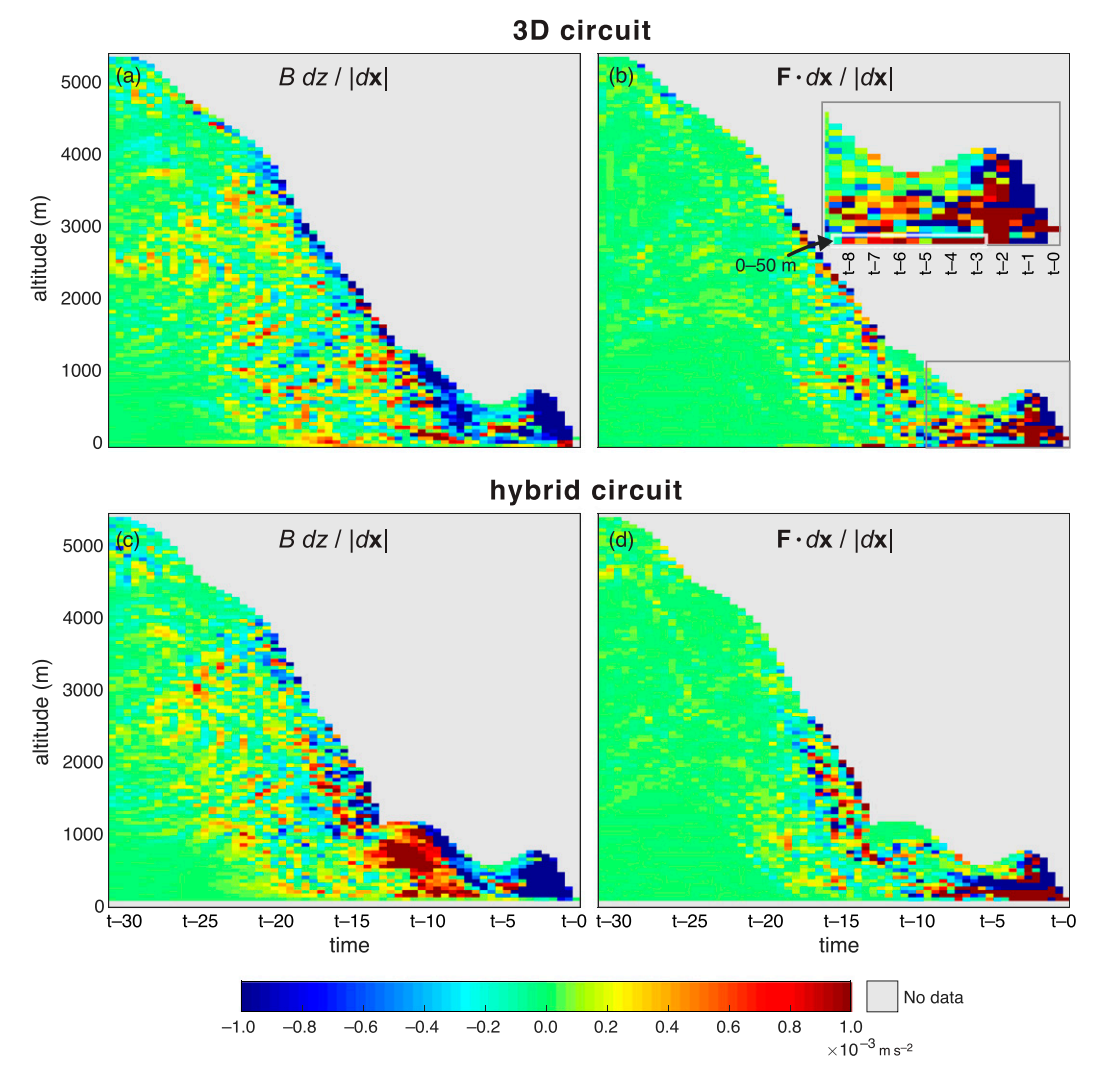


FIG. 10. Heat maps of normalized baroclinic and viscous circulation forcing $(Bdz/|d\mathbf{x}|$ and $\mathbf{F} \cdot d\mathbf{x}/|d\mathbf{x}|$, respectively) as a function of time and height for the (a),(b) 3D material and (c),(d) hybrid circuits. The forcings have been averaged in bins that are 50 m in depth and 30 s in duration. "No data" indicates an absence of parcels within a given time-height bin. The inset in (b) enlarges the portion of the plot in which there is a large positive (and suspect) forcing from turbulent and numerical diffusion along portions of the circuit that have dipped below the lowest scalar level (50 m; enclosed by the white-outlined rectangle).

Lewellen 1993). [See sections 4.1 and 6.2 of Davies-Jones (2015) for a brief synopsis of this mechanism].

6. Conclusions

To diagnose the origins of large vertical vorticity near the ground, supercell modelers calculate the circulation around material circuits. This approach suffers from the problem that trajectories become ill defined when parcels dip below the lowest scalar level of a staggered grid. To circumvent this problem, we derive (1), which provides the theorem for the rate of change of circulation around any moving closed curve. Special cases include a stationary curve, a material one, and a permanently horizontal one that is moving with the horizontal wind. To avoid having circuit parcels that dip below the lowest scalar level, we adopt a hybrid curve with material segments

used at heights $z \ge \Delta z$ and horizontal segments at $z = \Delta z$ where the material curve dips below $z = \Delta z$. Another force circulation has to be added to the customary equation for circulation [see (12)]. This force circulation is $\oint \mathbf{G} \cdot d\mathbf{x}$, where $\mathbf{G} = -w\partial_z \mathbf{v}_H$ is the force needed to keep the horizontal segments level and $\mathbf{G} = \mathbf{0}$ on the unrestrained parts of the circuit.

The generalized circulation theorem is verified through application to simple flows such as the development of updraft rotation in a sheared environment, flow around a bend, and vortex formation in axisymmetric flow. The hybrid-circuit method significantly improves the accuracy of the circulation budget in an idealized supercell simulation.

Acknowledgments. The second author received partial support from NSF Grant AGS-1821885. Doctor Harold Brooks

and the three anonymous reviewers are thanked for their insightful and thorough reviews that led to substantial improvements in the paper.

APPENDIX A

Rigorous Derivation of the Circulation Formula in (1)

Consider the circulation around any simple time-dependent closed curve K(t) in a reference frame rotating with Earth. The curve can be stationary or moving in any specified way in two or three dimensions. At a chosen initial time t = 0, the curve $K(\theta)$ can be parameterized by arc length s measured counterclockwise from an arbitrary point on the curve where s = 0. At later times s, the *initial* arc length, acts as a label for each curve point. On the curve there are two different velocity fields, namely, the wind $\mathbf{v}(s,t) \equiv [u(s,t), v(s,t)]$ t), w(s, t) at the curve points and the prescribed velocity $V(s,t) \equiv [U(s,t), V(s,t), W(s,t)]$ with which the curve points are moving. These velocity fields are the same only if the curve is a material one. In Cartesian coordinates let $\mathbf{x}(s, t) \equiv$ [x(s, t), y(s, t), z(s, t)] be the position vectors of the curve points. Then the velocity vector of the curve points is given by

$$\mathbf{V}(s,t) = \left[\frac{\partial \mathbf{x}(s,t)}{\partial t} \right]_{s}.$$
 (A1)

The nonadvective velocity of each curve point is $\mathbf{N}(s, t) = \mathbf{V}(s, t) - \mathbf{v}(s, t)$. On an f plane, the absolute circulation $\Gamma_a(t)$ around a closed curve K(t) is

$$\Gamma_{a}(t) = \oint\limits_{K(0)} \left[\mathbf{v}(s,t) + \frac{f}{2} \mathbf{k} \times \mathbf{x}(s,t) \right] \cdot \frac{\partial \mathbf{x}(s,t)}{\partial s} ds, \tag{A2}$$

where the quantity inside the square brackets is the absolute velocity (aside from a constant term that does not contribute to the contour integral). Note that line integrals with respect to s are along the curve K(0) and not K(t). The rate of change of circulation is therefore

$$\frac{\delta\Gamma_a}{\delta t} = \oint\limits_{K(0)} \left[\left(\frac{\partial \mathbf{v}}{\partial t} \right)_s + \frac{f}{2} \mathbf{k} \times \mathbf{V}(s, t) \right] \cdot \frac{\partial \mathbf{x}(s, t)}{\partial s} ds
+ \oint\limits_{K(0)} \left[\mathbf{v}(s, t) + \frac{f}{2} \mathbf{k} \times \mathbf{x}(s, t) \right] \cdot \frac{\partial \mathbf{V}(s, t)}{\partial s} ds$$
(A3)

with use of (A1). The line integrals of exact differentials around *closed* curves in a simply connected region vanish. By integration by parts with respect to *s* and use of the above property where applicable, we find that

$$\oint_{K(0)} \mathbf{v}(s,t) \cdot \frac{\partial \mathbf{V}(s,t)}{\partial s} ds = -\oint_{K(0)} \mathbf{N}(s,t) \cdot \frac{\partial \mathbf{v}(s,t)}{\partial s} ds \quad \text{and} \quad (A4)$$

$$\oint_{K(0)} \frac{f}{2} \mathbf{k} \times \mathbf{x}(s,t) \cdot \frac{\partial \mathbf{V}(s,t)}{\partial s} ds = \oint_{K(0)} \frac{f}{2} \left[-y(s,t) \frac{\partial U(s,t)}{\partial s} + x(s,t) \frac{\partial V(s,t)}{\partial s} \right] ds = \oint_{K(0)} \frac{f}{2} \left[U(s,t) \frac{\partial y(s,t)}{\partial s} - V(s,t) \frac{\partial x(s,t)}{\partial s} \right] ds$$

$$= \oint_{K(0)} \frac{f}{2} [\mathbf{k} \times \mathbf{V}(s,t)] \cdot \frac{\partial \mathbf{x}(s,t)}{\partial s} ds. \tag{A5}$$

Thus (A3) becomes

$$\frac{\delta\Gamma_{a}}{\delta t} = \oint\limits_{K(0)} \left(\frac{\partial \mathbf{v}}{\partial t}\right)_{s} \cdot \frac{\partial \mathbf{x}(s,t)}{\partial s} ds - \oint\limits_{K(0)} \mathbf{N}(s,t) \cdot \frac{\partial \mathbf{v}(s,t)}{\partial s} ds + \oint\limits_{K(0)} [f\mathbf{k} \times \mathbf{V}(s,t)] \cdot \frac{\partial \mathbf{x}(s,t)}{\partial s} ds. \tag{A6}$$

To proceed further we need to ascertain the meaning of $(\partial \mathbf{v}/\partial t)_s$. In terms of Cartesian coordinates,

$$\mathbf{v}(s,t) = \hat{\mathbf{v}}[x(s,t), y(s,t), z(s,t), t], \tag{A7}$$

where $\hat{\mathbf{v}}$ is the wind reexpressed as an explicit function of x, y, z. Hence.

$$\left(\frac{\partial \mathbf{v}}{\partial t}\right)_{s} = \left(\frac{\partial \hat{\mathbf{v}}}{\partial t}\right)_{x,y,z} + \left(\frac{\partial \hat{\mathbf{v}}}{\partial x}\right)_{y,z,t} \left(\frac{\partial x}{\partial t}\right)_{s} + \left(\frac{\partial \hat{\mathbf{v}}}{\partial y}\right)_{x,z,t} \left(\frac{\partial \mathbf{y}}{\partial s}\right)_{s} + \left(\frac{\partial \hat{\mathbf{v}}}{\partial z}\right)_{x,z,t} \left(\frac{\partial \mathbf{z}}{\partial t}\right)_{s} = \left(\frac{\partial \hat{\mathbf{v}}}{\partial t}\right)_{x,y,z} + (\mathbf{V} \cdot \nabla)\hat{\mathbf{v}} = \frac{d\hat{\mathbf{v}}}{dt} + (\mathbf{N} \cdot \nabla)\hat{\mathbf{v}} \tag{A8}$$

by (A1), where $d\hat{v}/dt$ is the material derivative of **v** in the rotating reference frame. Differentiating (A7) with respect to *s* yields

$$\left(\frac{\partial \mathbf{v}}{\partial s}\right)_{t} = \frac{\partial \hat{v}}{\partial x} \left(\frac{\partial x}{\partial s}\right)_{t} + \frac{\partial \hat{v}}{\partial y} \left(\frac{\partial y}{\partial s}\right)_{t} + \frac{\partial \hat{v}}{\partial z} \left(\frac{\partial z}{\partial s}\right)_{t} = \nabla \hat{v} \cdot \left(\frac{\partial \mathbf{x}}{\partial s}\right)_{t}.$$
(A9)

Inserting (A8) and (A9) into (A6) and discarding the now unnecessary hat (caret) notation yields

$$\frac{\delta\Gamma_{a}}{\delta t} = \oint\limits_{K(t)} \left[\frac{d\mathbf{v}}{dt} + f\mathbf{k} \times \mathbf{v} + (\mathbf{N} \cdot \nabla)\mathbf{v} - \mathbf{N} \cdot \nabla\mathbf{v} + f\mathbf{k} \times \mathbf{N} \right] \cdot d\mathbf{x},$$
(A10)

where

$$\mathbf{N} \cdot \nabla \mathbf{v} = N_i \partial v_i / \partial x_i \tag{A11}$$

in tensor notation. With the aid of a vector identity

$$(\mathbf{N} \cdot \nabla)\mathbf{v} - \mathbf{N} \cdot \nabla \mathbf{v} = (\nabla \times \mathbf{v}) \times \mathbf{N} \tag{A12}$$

(D'haeseleer et al. 1991, p. 39), (A10) becomes

$$\frac{\delta\Gamma_a}{\delta t} = \oint\limits_{K(t)} \left[\frac{d\mathbf{v}}{dt} + f\mathbf{k} \times \mathbf{v} + (\nabla \times \mathbf{v}) \times \mathbf{N} + f\mathbf{k} \times \mathbf{N} \right] \cdot d\mathbf{x}. \quad (A13)$$

From the vector equation of motion on an f plane,

$$\frac{d\mathbf{v}}{dt} + f\mathbf{k} \times \mathbf{v} = -\alpha \nabla p - \nabla (gz) - gq_l \mathbf{k} + \mathbf{F}.$$
 (A14)

Introducing (A14) into (A13) gives

$$\frac{\delta\Gamma_a}{\delta t} = \oint\limits_{K(t)} (\boldsymbol{\omega}_a \times \mathbf{N}) \cdot d\mathbf{x} - \oint\limits_{K(t)} \alpha \, dp - g \oint\limits_{K(t)} q_t \, dz + \oint\limits_{K(t)} \mathbf{F} \cdot d\mathbf{x},$$
(A1)

which is the circulation theorem in (1).

APPENDIX B

Line-Segment Theorem for a Material Curve

Here we consider the line integral around a curve C(t), which is just a material segment of a closed material circuit K(t), and we set f = 0 for simplicity. Since C(t) and K(t) are material curves, $\mathbf{V} = \mathbf{v}$ and $\mathbf{N} = \mathbf{0}$. Arclength s along the initial circuit K(0) labels the parcels on the material curves. Let s_1 and s_2 be the endpoint labels of the material segment. The contribution I(t) from the material segment to the circulation around the material circuit is

$$I(t) = \int_{s}^{s_2} \mathbf{v}(s,t) \cdot \frac{\partial \mathbf{x}(s,t)}{\partial s} ds.$$
 (B1)

The material rate of change of I is

$$\frac{dI}{dt} = \int_{s_1}^{s_2} \frac{\partial \mathbf{v}(s,t)}{\partial t} \cdot \frac{\partial \mathbf{x}(s,t)}{\partial s} ds + \int_{s_1}^{s_2} \mathbf{v}(s,t) \cdot \frac{\partial \mathbf{v}(s,t)}{\partial s} ds.$$
 (B2)

On a material curve $(\partial \mathbf{v}/\partial t)_s$ is simply $d\mathbf{v}/dt$, however. Therefore,

$$\frac{dI}{dt} = \int_{s_1}^{s_2} \frac{d\mathbf{v}}{dt} \cdot d\mathbf{x} + \left(\frac{\mathbf{v} \cdot \mathbf{v}}{2}\right)_{s_1}^{s_2}.$$
 (B3)

Inserting the equation of motion in the form

$$\frac{d\mathbf{v}}{dt} = T\nabla S - \nabla(c_p T + gz) - gq_l \mathbf{k} + \mathbf{F}, \tag{B4}$$

where S is entropy, gives

$$\frac{dI}{dt} = \int_{s_1}^{s_2} T \, dS - \int_{s_1}^{s_2} g q_l \, dz + \int_{s_1}^{s_2} \mathbf{F} \cdot d\mathbf{x} + \left(\frac{\mathbf{v} \cdot \mathbf{v}}{2} - c_p T - gz\right)_{s_1}^{s_2},$$
(B5)

where $(\mathbf{v} \cdot \mathbf{v})/2 - c_p T - gz$ is the specific kinetic energy of a parcel minus its specific enthalpy and specific potential energy. The last term in (B5) originates from an irrotational wind

component. It is zero for a closed circuit ($s_1 = s_2$) in a simply connected region. Parcels entering a tornado gain kinetic energy and lose enthalpy (Davies-Jones 2015, section 6.2). Even though the barotropic circulation around the entire material circuit is constant, the contribution to barotropic-circulation gain from a material segment will increase significantly if the segment is drawn lengthwise into a tornado.

Using the Boussinesq-approximated form of the equation of motion instead of (B4) yields

$$\frac{dI}{dt} = \int_{s_1}^{s_2} B \, dz + \int_{s_1}^{s_2} \mathbf{F} \cdot d\mathbf{x} + \left(\frac{\mathbf{v} \cdot \mathbf{v}}{2} - \alpha_0 p'\right)_{s_1}^{s_2}, \tag{B6}$$

where the first two terms on the right are the work done by buoyancy and frictional forces on a hypothetical parcel that moves instantaneously along the curve segment from s_1 to s_2 . The third term on the right is the specific kinetic energy minus specific pressure energy. It increases rapidly with proximity to a vortex.

REFERENCES

Adlerman, E. J., K. K. Droegemeier, and R. P. Davies-Jones, 1999: A numerical simulation of cyclic mesocyclogenesis. *J. Atmos. Sci.*, **56**, 2045–2069, https://doi.org/10.1175/1520-0469(1999) 056<2045:ANSOCM>2.0.CO;2.

Bluestein, H. B., K. J. Thiem, J. C. Snyder, and J. B. Houser, 2019: Tornadogenesis and early Tornado evolution in the El Reno, Oklahoma, supercell on 31 May 2013. *Mon. Wea. Rev.*, **147**, 2045–2066, https://doi.org/10.1175/MWR-D-18-0338.1.

Dahl, J. M. L., 2015: Near-ground rotation in simulated supercells: On the robustness of the baroclinic mechanism. *Mon. Wea. Rev.*, **143**, 4929–4942, https://doi.org/10.1175/MWR-D-15-0115.1.

—, M. D. Parker, and L. J. Wicker, 2012: Uncertainties in trajectory calculations within near-surface mesocyclones of simulated supercells. *Mon. Wea. Rev.*, **140**, 2959–2966, https:// doi.org/10.1175/MWR-D-12-00131.1.

—, —, and —, 2014: Imported and storm-generated nearground vertical vorticity in a simulated supercell. *J. Atmos. Sci.*, **71**, 3027–3051, https://doi.org/10.1175/JAS-D-13-0123.1.

Davies-Jones, R., 1984: Streamwise vorticity: The origin of updraft rotation in supercell storms. J. Atmos. Sci., 41, 2991–3006, https:// doi.org/10.1175/1520-0469(1984)041<2991:SVTOOU>2.0.CO;2.

—, 2004: Growth of circulation around supercell updrafts. J. Atmos. Sci., 61, 2863–2876, https://doi.org/10.1175/JAS-3341.1.

——, 2008: Can a descending rain curtain in a supercell instigate tornadogenesis barotropically? J. Atmos. Sci., 65, 2469–2497, https://doi.org/10.1175/2007JAS2516.1.

——, 2015: A review of supercell and tornado dynamics. *Atmos. Res.*, 158–159, 274–291, https://doi.org/10.1016/j.atmosres.2014.04.007.

—, and H. E. Brooks, 1993: Mesocyclogenesis from a theoretical perspective. *The Tornado: Its Structure, Dynamics, Prediction,* and Hazards, Geophys. Monogr., Vol. 79, Amer. Geophys. Union, 105–114.

—, and V. T. Wood, 2006: Simulated Doppler velocity signatures of evolving tornado-like vortices. *J. Atmos. Oceanic Technol.*, 23, 1029–1048, https://doi.org/10.1175/JTECH1903.1.

——, R. J. Trapp, and H. B. Bluestein, 2001: Tornadoes and tornadic storms. Severe. Convective Storms, Meteor. Monogr., No. 50, 167–222, https://doi.org/10.1175/0065-9401-28.50.167.

- D'haeseleer, W. D., W. N. G. Hitchon, J. D. Callen, and J. L. Shohet, 1991: *Flux Coordinates and Magnetic Field Structure*. Springer-Verlag, 241 pp.
- Dombre, T., U. Frisch, J. M. Greene, M. Henon, A. Mahr, and A. M. Soward, 1986: Chaotic streamlines in the ABC flows. *J. Fluid Mech.*, 167, 353–391, https://doi.org/10.1017/S0022112086002859.
- Dutton, J. A., 1986: The Ceaseless Wind. Dover, 617 pp.
- Fiedler, B. H., and R. Rotunno, 1986: A theory for the maximum windspeed in tornado-like vortices. *J. Atmos. Sci.*, **43**, 2328–2340, https://doi.org/10.1175/1520-0469(1986) 043<2328:ATOTMW>2.0.CO;2.
- Fujita, T. T., 1973; Proposed mechanism of tornado formation from rotating thunderstorm. Preprints, *Eighth Conf. on Severe Local Storms*, Denver, CO, Amer. Meteor. Soc., 191–196.
- Glaser, A. H., 1960: An observational deduction of the structure of a tornado vortex. *Cumulus Dynamics*, C. Anderson, Ed., Pergamon Press, 157–166.
- Hoecker, W. H., 1960: Wind speed and air flow patterns in the Dallas tornado of April 2, 1957. Mon. Wea. Rev., 88, 167–180, https:// doi.org/10.1175/1520-0493(1960)088<0167:WSAAFP>2.0.CO;2.
- Lewellen, S., 1993: Tornado vortex theory. The Tornado: Its Structure, Dynamics, Prediction, and Hazards, Geophys. Monogr., Vol. 79, Amer. Geophys. Union, 19–39.
- Lilly, D. K., 1982: The development and maintenance of rotation in convective storms. *Intense Atmospheric Vortices*, L. Bengtsson and J. Lighthill, Eds., Springer-Verlag, 149–160.
- Mandelbrot, B. B., 1982: *The Fractal Geometry of Nature*. W. H. Freeman and Company, 480 pp.
- Markowski, P. M., 2016: An idealized numerical simulation investigation of the effects of surface drag on the development of near-surface vertical vorticity in supercell thunderstorms. J. Atmos. Sci., 73, 4349–4385, https://doi.org/10.1175/JAS-D-16-0150.1.
- —, and Y. P. Richardson, 2014: The influence of environmental low-level shear and cold pools on tornadogenesis: Insights from idealized simulations. *J. Atmos. Sci.*, 71, 243–275, https:// doi.org/10.1175/JAS-D-13-0159.1.
- —, J. M. Straka, and E. N. Rasmussen, 2003: Tornadogenesis resulting from the transport of circulation by a downdraft: Idealized numerical simulations. *J. Atmos. Sci.*, 60, 795–823, https://doi.org/10.1175/1520-0469(2003)060<0795:TRFTTO>2.0.CO;2.
- —, and Coauthors, 2012: The pretornadic phase of the Goshen County, Wyoming, supercell of 5 June 2009 intercepted by VORTEX2. Part II: Intensification of low-level rotation. *Mon. Wea. Rev.*, **140**, 2916–2938, https://doi.org/10.1175/MWR-D-11-00337.1.
- ——, N. T. Lis, D. D. Turner, T. R. Lee, and M. S. Buban, 2019: Observations of near-surface vertical wind profiles and vertical momentum fluxes from VORTEX-SE 2017: Comparisons

- to Monin-Obukhov similarity theory. *Mon. Wea. Rev.*, **147**, 3811–3824, https://doi.org/10.1175/MWR-D-19-0091.1.
- Morton, B. R., 1966: Geophysical vortices. *Prog. Aeronaut. Sci.* **7**, 145–193, https://doi.org/10.1016/0376-0421(66)90008-X.
- Orf, L., R. Wilhelmson, B. Lee, C. Finley, and A. Houston, 2017: Evolution of a long-track violent tornado within a simulated supercell. *Bull. Amer. Meteor. Soc.*, 98, 45–68, https://doi.org/ 10.1175/BAMS-D-15-00073.1.
- Roberts, B., and M. Xue, 2017: The role of surface drag in mesocyclone intensification leading to tornadogenesis within an idealized supercell simulation. *J. Atmos. Sci.*, **74**, 3055–3077, https://doi.org/10.1175/JAS-D-16-0364.1.
- —, —, A. D. Schenkman, and D. T. Dawson, 2016: The role of surface drag in tornadogenesis within an idealized supercell simulation. *J. Atmos. Sci.*, **73**, 3371–3495, https://doi.org/ 10.1175/JAS-D-15-0332.1.
- ——, and D. T. Dawson, 2020: The effect of surface drag strength on mesocyclone intensification and tornadogenesis in idealized supercell simulations. *J. Atmos. Sci.*, 77, 1699–1721, https://doi.org/10.1175/JAS-D-19-0109.1.
- Rott, N., 1958: On the viscous core of a line vortex. *Z. Angew. Math. Phys.*, **9**, 543–553, https://doi.org/10.1007/BF02424773.
- Rotunno, R., 1986: Tornadoes and tornadogenesis. Mesoscale Meteorology and Forecasting, P. S. Ray, Ed., Amer. Meteor. Soc., 414–436.
- —, and J. B. Klemp, 1985: On the rotation and propagation of simulated supercell thunderstorms. *J. Atmos. Sci.*, 42, 271–292, https://doi.org/10.1175/1520-0469(1985)042<0271:OTRAPO> 2.0.CO;2.
- Shapiro, A. H., 1972: Vorticity. *Illustrated Experiments in Fluid Mechanics: The NCFMF Book of Film Notes*, MIT Press, 63–74, http://web.mit.edu/hml/ncfmf/09VOR.pdf.
- Tao, T., and T. Tamura, 2020: Numerical study of the 6 May 2012 Tsukuba supercell tornado: Vorticity sources responsible for tornadogenesis. *Mon. Wea. Rev.*, 148, 1205–1228, https:// doi.org/10.1175/MWR-D-19-0095.1.
- Trapp, R. J., and B. H. Fiedler, 1995: Tornado-like vortexgenesis in a simplified numerical model. *J. Atmos. Sci.*, **52**, 3757–3778, https://doi.org/10.1175/1520-0469(1995)052<3757:TLVIAS> 2.0.CO;2.
- —, and M. L. Weisman, 2003: Low-level mesovortices within squall lines and bow echoes. Part II: Their genesis and implications. *Mon. Wea. Rev.*, 131, 2804–2823, https://doi.org/10.1175/1520-0493(2003)131<2804:LMWSLA>2.0.CO;2.
- Yokota, S., H. Niino, H. Seko, M. Kunii, and H. Yamauchi, 2018: Important factors for tornadogenesis as revealed by highresolution ensemble forecasts of the Tsukuba supercell tornado of 6 May 2012 in Japan. Mon. Wea. Rev., 146, 1109–1132, https://doi.org/10.1175/MWR-D-17-0254.1.